DOTTORATO DI RICERCA IN
Scienze Anestesiologiche e Chirurgiche

CICLO XXXII

COORDINATORE Prof. Marco Matucci Cerinic

Sviluppo di un sistema di coagulazione a microonde per l'impiego in chirurgia epatica mininvasiva e robotica

Settore Scientifico Disciplinare MED/18

Dottorando
Dott. Fabio Staderini

Tutore
Prof. Fabio Cianchi

Coordinatore
Prof. Marco Matucci Cerinic

Anni 2016/2019

ABSTRACT

During the last two decades, many surgical procedures have been evolved from traditional open surgery to less invasive or minimally invasive surgery. This limited invasiveness has motivated the development of robotic assistance platforms used during the surgical intervention to obtain better surgical outcomes. Nowadays, the da Vinci robotic system is the commercial robotic platform mostly used for modern minimally invasive surgical applications. Even in the field of minimally invasive hepatic surgery the Da Vinci Platform has been used, but not widely as in other organs such as prostate or lower rectum. The reason of this low spread needs to be researched in many factors. One of the most important is the difficulty in bleeding control during hepatic robotic surgery. Bleeding from parenchyma transection during a robotic hepatic surgery in fact remains one of the most critical point affecting the low spread of hepatic robotic surgery and also affecting the postoperative recovery and long-term survival. In order to solve this problem various robotic devices with different types of energies have been proposed; however, each of these commercially available robotic tools lack in steerability, efficacy, or accuracy. The aim of this work was to "de-novo" project and evaluate the feasibility and performance of a new steerable microwave resection device (SMRD) intended for minimizing intraoperative blood loss during robotic liver resections. The new device operating at 2.45 GHz has been designed to accommodate the engineering constraints derived from its use for robotic surgery, in which a steerable head is required and the internal cooling of forced gas or water is undesirable. The device project, design, analysis, and optimization were addressed using the most advanced commercial electromagnetic and thermal solvers to achieve the best results. To experimentally validate the results of the numerical analysis, many ablations were performed on freshly explanted bovine liver by using a single device prototype with three levels of energy supplied to the tissue. During the ablation procedures, the time, temperature, and shape of the thermal lesion were recorded using thermocouples and an infrared thermos-camera.

Ex vivo tests showed good agreement with the numerical simulations, demonstrating the validity of the simplifications adopted to deal with the complex phenomena involved in the extreme hyperthermia of a living tissue. The high performance, thermal reliability, and robustness of the developed device were also demonstrated along with the possibility of reducing operation time and blood loss. In this work, the da Vinci Research Kit (dVRK), namely the research version of the commercial da Vinci robotic platform, was used to manipulate the novel microwave device in a teleoperation scenario. The dVRK provides an open source hardware/software platform, so that the novel microwave tool, dedicated to hepatic prevention bleeding during hepatic resection surgery, was mechanically integrated on the slave side, while consistently the software interface was adapted in order to correctly control tool pose. Tool integration and control were validated through in-vitro and ex-vivo tests, meanwhile the coagulative efficacy of the developed tool in a perfused liver model has been proved during in-vivo test session. In conclusion, an innovative microwave (MW) tool for liver robotic resection has been realized and integrated into a commercially available surgical robot. The tool can be easily operated through the dVRK master console without limiting the intuitive and friendly use, and thus easily reaching the hemostasis of liver vessels.

KEYWORDS

microwave device, da Vinci Research Kit, thermal ablation, robotic surgery, minimally invasive surgery

PUBLICATIONS

1) **Staderini F**., Frosini F., Brancadoro M., Dimitri M., Regolini J., BoushakiM.N., Vegni A., Coratti A., Biffi Gentili G., Cianchi F. - Development of a robotic pre-coagulation device for hepatic surgery. CRSA Clinical Robotic Association, Chicago 22-23 Sept. 2017

2) F. Frosini, **F. Staderini**, M. Brancadoro, M. Dimitri, J. Regolini1, R. Miniati, M.N. Boushaki, L. Paternò, F. Guerra, A. Coratti, F. Cianchi, A. Corvi, A. Menciassi, G. Biffi Gentili - *A novel microwaves tool for robotic resection of the liver*

iSMIT Conference of the international Society for Medical Innovation and Technology

Turin 9 - 10 November 2017

3) Dimitri M, **Staderini F**, Brancadoro M,Frosini F,Coratti A,Capineri L,Corvi A,Cianchi F,Biffi Gentili G. - *A new microwave applicator for laparoscopic and robotic liver resection*

Int J Hyperthermia. 2019;36(1):75-86

4) **Staderini F** -*A novel microwave tool for the robotic resection of the liver*

PhDday UniFi 23/5/2019

5) M. Brancadoro, M. Dimitri, M. N. Boushaki, **F. Staderini**, E. Sinibaldi, L. Capineri, F. Cianchi, G. Biffi Gentili and A. Menciassi - *A Novel Microwave Tool for the Liver Robotic Resection in Minimally Invasive Surgery*

Manuscript under revision at: Minimally Invasive Therapy & Allied Technologies Journal

INTRODUCTION

Hepatocellular carcinoma accounts for about 80% of all primitive hepatic cancers. It is the sixth most commonly diagnosed cancer in the world [1, 2]. Despite the improvements in surgical techniques and the technological advancements for liver resection, intraoperative bleeding remains the most critical issue which negatively affects postoperative course and survival [3]. During hepatic surgery the bleeding rate is very variable, depending on the type of surgical technique and the patient's general conditions. In open surgery, with the clamp crush technique, mean estimated blood loss ranges from 700 ml to 1200 ml, with the surgical death ranging from 4% to 5% as reported by Aldrighetti et al. [4]. This data underlines the importance of bleeding prevention during hepatic surgery.

In order to avoid bleeding related problems, thermal percutaneous ablation (TPA) is used by some authors to treat with minimal invasiveness neoplastic nodules up 30 mm in diameter [4-6]. Percutaneous thermal ablation is a non surgical procedure that uses an energy source (either heat, cold, or chemical) to destroy cancerous tissue in a target organ. This procedure involves advancing a special type of needle directly into the tumor within the target organ with the assistance of US, CT scan and/or X-ray guidance (Fig1). The needle is used to deliver an energy source to the tumor to destroy it while minimizing damage in the target organ.

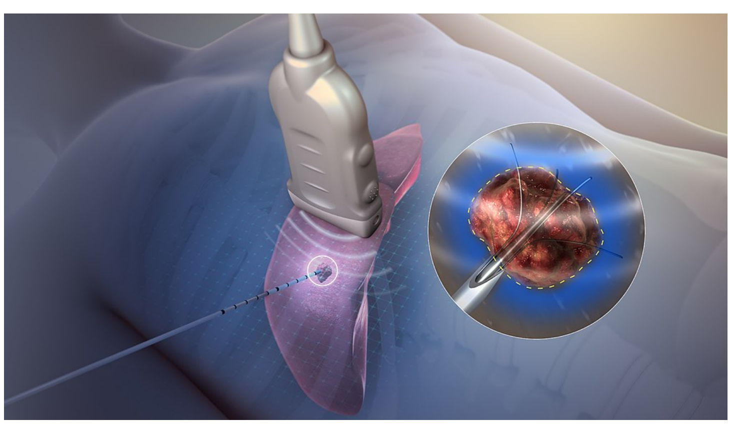

Fig. 1 Percutaneous RF ablation of a liver tumor

Except for special situations such, neoplasia located in unresectable locations, high number of lesions, inadequate hepatic reserve or multiple comorbidities that contraindicates anaesthesia, this technique is still not considered the gold standard as liver transplant and hepatic resection have proven their superiority in treating primary and secondary hepatic neoplasms. Surgery and hepatic transplant in fact have demonstrated superior long-term disease-free survival rates when compared with TPA [6]. Moreover, several studies [7–10] have underlined the importance of surgical resection, and a recent study has suggested that the indication for hepatic resection could be further extended by improving diagnostic methods, surgical skills and developing advanced technologies as robotic platforms.

As the majority of liver interventions are still conducted with traditional open technique, the solution to intraoperative bleeding control is considered of fundamental importance because the spreading of robotic minimally invasive surgery could also solve the difficult postoperative recovery of the patients operated with traditional open-surgery technique. As a consequence of that, various techniques and instruments have been developed to minimize bleeding during minimally invasive liver resections. In this framework, there is an increasing interest of the research community towards dedicated solutions for bleeding reduction. Dedicated devices have been developed not only by universities and medical centres, but also by active medical device corporations with broad market possibilities [6]. Some examples include Ultracision harmonic scalpel (Johnson and Johnson Medical SpA, U.S.), Vessel Sealer (Intuitive Surgical Inc, Sunnyvale, CA), Cavitron Ultrasonic Surgical Aspirator, CUSA (Valleylab Inc., U.S.), Bipolar Cautery Forceps(Intuitive Surgical Inc, Sunnyvale, CA)) and Habib 4X Laparoscopic Bipolar Resection Device (AngioDynamics Inc., U.S.) (Fig.2). However, each of these commercially available robotic tools have several drawback. Someone lack in steerability, someone in efficacy, someone in accuracy.

Fig 2. Commercially available robotic/laparoscopic instruments for bledding control during hepatic surgery.

Hepatectomy using coagulative necrosis (HCN) is a minimally invasive surgical technique that has been developed to avoid these bleeding-related problems. Curro et al. [11] was the first to report on the use of a radiofrequency (RF) device (Habib 4X, RITA Medical System, Mountain View, United States) to precoagulate the resection line before starting to dissect the liver (Fig 3). The basic principle of liver resection line procoagulation consists of creating a non-perfused zone using very high temperature hyperthermia (around 80°C) along the surgical resection line[5].

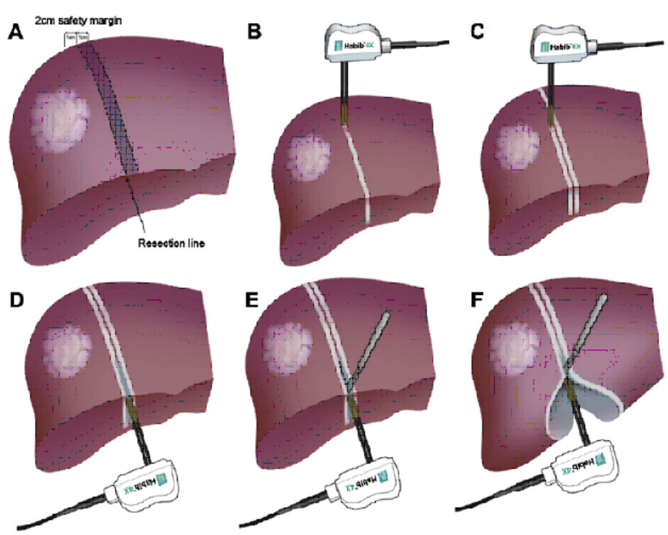

Fig 3. Habib technique of liver resection

After the first report of Curro et al several studies confirmed the usefulness of this technique [12–13]. Concerning HCN and focusing on research products, the state of the art proposes the Radio Frequency (RF) principle as a stable, safe and promising solution for hepatectomy [7].

In the field of hepatic neoplasms, RF technology, having the longest history among thermal ablation methods, is the most frequently used energy in both percutaneous and heat coagulative necrosis use [8]. Most HCN devices use RF technology because it is simple, relatively low cost and easy to use. However, several drawbacks have been associated with the RF technique. The first one is related to RF energy itself as it is a high voltage current that passes from the device electrode to the ground pad under the patient's back, thus carrying on the risk of patient skin burning, myocardial infarction and arrhythmias. In addition, the electrical currents are randomly distributed along the patient's body, thus the shape and dimensions of the RF coagulation zone are not so predictable. Moreover, the RF approach is time-consuming if compared to the other types of hyperthermia energies [9]. Microwaves (MW), despite their complexity and costs, present several theoretical advantages if compared to RF and to all the others type of hyperthermia energies [14-15]. Unlike RF ablation, the energy penetration of MW during ablation procedures (MWA) is not affected by the electrical conductivity and permittivity of tissue. Moreover, the MWA reaches higher temperatures, has less severe heat sink effects, shorter ablation time, larger ablation zone and no need of ground pads [16].

Due to this advantages the rapid progress in MW technology has recently attracted considerable attention in the development and optimization of internally cooled [15] and not internally cooled [17] MW devices for the percutaneous MWA of liver tumors. Unfortunately, the development of new technologically advanced MW devices specifically intended for laparoscopic and robot-assisted MW coagulation procedures [18] has received less attention. Liver resection using MTC has not yet become widespread because a simple, safe, and effective uncooled MW device useful for laparoscopic and robotic surgery is yet to be produced.

In the field of hepatic surgery, even if hepatic transplant is the ideal technique[19], it is far from being the optimal procedure because it is very demanding, needs liver donors and the failure rate is still not negligible. On the contrary, open surgical resection is easier and more widespread, but in the current clinical panorama where surgery is going toward a reduction of patient trauma, open surgery should not be considered the future of liver surgery. In fact, all surgical techniques have experienced an evolution from traditional open surgery to minimally invasive surgery (MIS) especially laparoscopic surgery. This evolution has witnessed an improvement of the surgical outcomes thanks to the limitation of the patient body incisions*,* reduced patient trauma, less blood-loss and shorter recovery duration. However, remarkable limitations are associated to laparoscopic technique(Fig 4). The accessibility to the surgical target requires the passage through complex 3D paths and the control of the surgical instruments is more difficult (*e.g.,* constrained manipulability, less dexterity and degrees of freedom - DoF) [20].

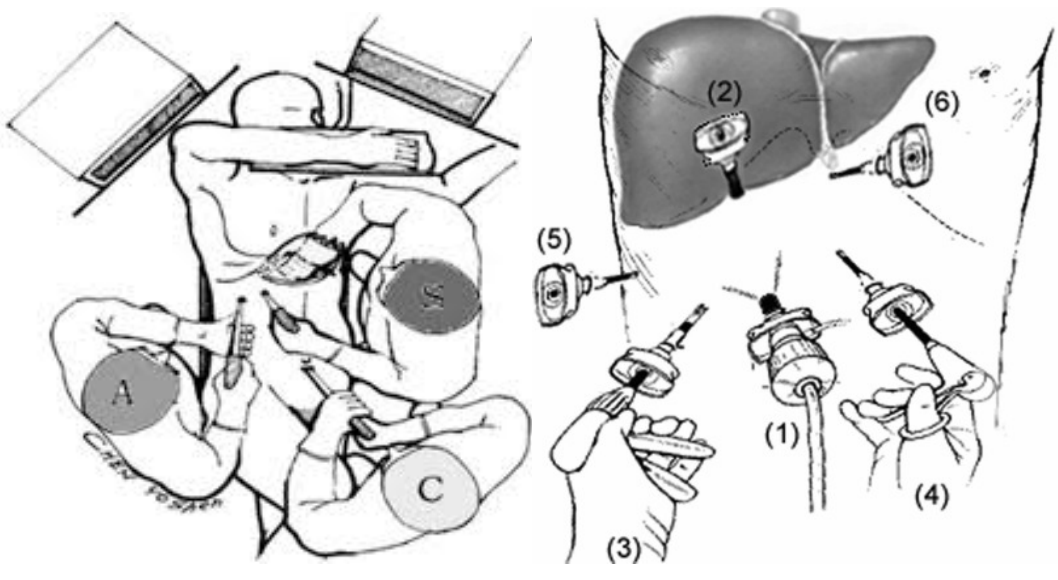

Fig 4. Laparoscopic liver surgery technique and operative setup

These limitations have motivated the use of robotic assistance for better benefits in MIS. Robotic surgery has been introduced to overcome some of this technical limitations of laparoscopic surgery, such as two-dimensional vision, amplified physiological tremor, restricted range of motion and ergonomic discomfort [21, 22]. Robotic systems include operator-controlled 3-dimensional cameras that ensure steady and effective surgical fields of view with motion scaling and multiple degrees of freedom(Fig5).

Fig 5. Da Vinci robotic platform

The da Vinci robotic platform consists of three components: the surgeon's console which directs the movements of the robotic arms (Fig 6), the vision system (Fig 7), the patient-side cart (Fig 8), which in the latest system has four arms.

Fig. 6

Fig 7

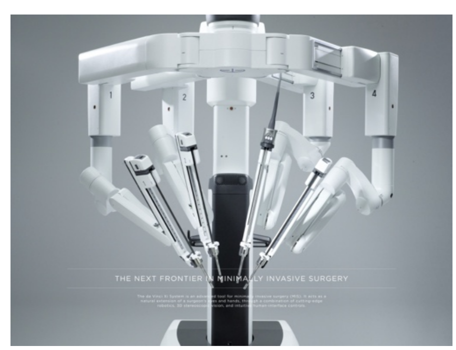

Fig 8

After the placement of port sites and docking the patient side cart, the surgeon sits at the console and is able to view the surgical field through a three-dimensional vision system in high definition. Furthermore, the camera system is stabilized by the robotic platform and easily controlled by the surgeon through foot pedals and arm movements. At the console, the surgeon controls the robotic arms and the EndoWrist instruments with natural hand and wrist motions that mimic movements performed in open surgery. In fact, the EndoWrist instruments are designed with seven degrees of freedom (Fig 9), one more than the human hand (e.g. wristed pitch).

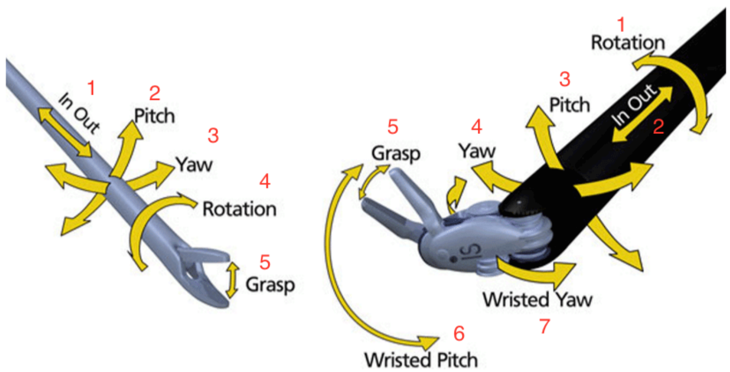

Fig 9. Comparison of a laparoscopic VS robotic instrument degrees of freedoms

Also, the robotic system is able to reduce tremor and is ergonomic for the surgeon with armrests and adjustable height and eye pieces. It also offers ease of use through foot pedals that control swapping in and out the third robotic arm, moving and focusing the camera, and controlling monopolar and bipolar currents connected to the EndoWrist instruments. All of these components reduce the fatigue, frustration, and strain experienced by laparoscopic surgeons during long or difficult cases.

Thanks to all the above advantages, the da Vinci Robotic System (Intuitive Surgical Inc, Sunnyvale, CA) is becoming more and more used in surgical interventions. More than 877,000 procedures have been performed in 2017 for multiple surgical disciplines, including general surgery, urology, gynecology, thoracic and trans-oral surgery. These procedures have been performed by using more than 4,400 da Vinci robotic platforms operating in hospitals and clinics around different countries [23]. Together with the commercial robotic platform the Intuitive Surgical has developed an open source research version of the da Vinci system that is nowadays available, and which has the same mechanical structure of the first da Vinci version associated with totally open source software platform [24]. This platform, called da Vinci Research Kit (dVRK), allows to modify all levels of the control software and integrating customised surgical devices (Fig 10).

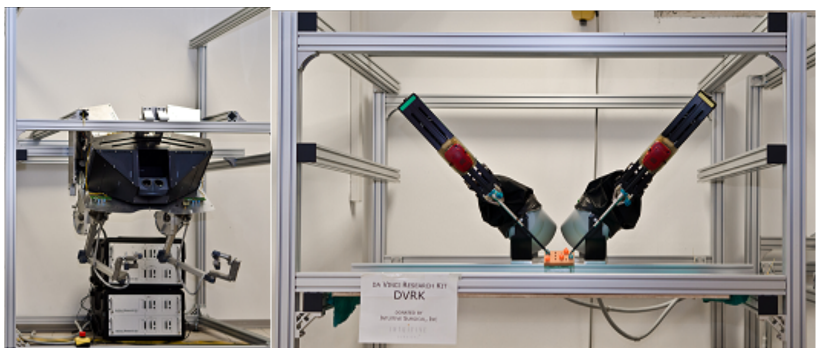

Fig 10. DvRK at the Bio-Robotic Institute, SSA, Pisa

The idea of robotizing the Hepatic Microwave Coagulation Therapy procedure has been introduced in [25]. A robotic surgery navigation system has been developed using a 5 DoF robot and a stereovision technique in order to reduce the effect of the physiological motions and then improve the MW needle insertion accuracy. Another approach has been used in [26] to improve MW needle placement accuracy using a 3D ultrasound image-guided system. These work has been extended by demonstrating automatic planning of robotically assisted multiple-needle insertions [27], with application to coagulation in large liver tumour therapy. Furthermore, in [28], an MR-compatible motorized portable robot has been designed to automatically reach the target point. Using this device, the liver tumour puncture has been performed under MR image guidance. In addition, several manual instruments have been designed for the same purpose from different research groups [29-35]. All these previous works, even if exploiting advanced mechanisms for improving needle placement and MW ablation performance, have not benefited from the advantages of any robotic surgical procedures.

The objectives of an ideal non-anatomical liver-resection procedure mainly involve the resection of the tumor by preserving a sufficient amount of free margin of healthy liver to guarantee oncological radicality and minimize intraoperative blood loss. In some cases, surgeons have tried to mutate the interventional radiology technique by using commercially available MW water- or gas-cooled needle applicators to produce sequential ablations along the transection line to precoagulate it in open surgery [36-38] with good results in blood-loss minimization. However, for laparoscopic and robotic MW liver resection, this applicator type does not represent the optimal solution because its tip is not steerable and the forced cooling requires a complicated mechanical pumping sub-system and a pair of connection tubes for fluid circulation.

Therefore, the main objective of this study was to design a new uncooled steerable MW applicator by optimizing its mechanical structure by using the most advanced electromagnetic and thermokinetic numerical simulators.

-*Primary endpoint* was to create an optimized MW coagulator that should be capable of the following:

1- creating a small non-perfused zone associated with permanent clot firmness and excellent thermal stability;
2- preventing excessive tissue heating and consequent hepatic damage due to lateral MW spreading;
3- at the end of the procedure, the device temperature should not exceed 70 °C so as to prevent internal organ damage during laparoscopic and robotic procedures.

-*Secondary endpoint* was to numerically and experimentally evaluate the feasibility of a new liver-transection device optimized both for safe robotic interventions, demonstrating that a well-designed and finalized device eases the procedure, reduces risks, and minimizes the operative time for a safe hepatectomy.

-Tertiary endpoint was to achieve hardware and software integration of the new MW robotic tool into the dVRK robotic platform, in order to experimentally prove its usability for liver bloodless robotic resection in a teleoperated MIS scenario. Ex-vivo and in-vivo tests was performed by surgical staff. Based on the obtained results, tool integration and overall functionality was evaluated.

MATERIALS AND METHODS

MW needle and MW system setup

The proposed MW device needed to be conceived specifically to follow the previous objectives of mechanical simplicity, thermal stability, and safety. We decided first that the MW system would have been projected without the internal cooling, in order to:

- reduce the system complexity.

-improve maneuverability

-ease the integration with laparoscopic and robotic tools into the surgical room

-lower the final cost of the device.

The ablation apparatus was designed by two main parts: a 2.45-GHz, 120-Watt MW generator designed by the Department of Information Engineering, University of Florence, and a laptop to set all the parameters of the ablation sequences. The device should have had, dimensions compatible with laparoscopic and robotic interventions, with a steerable head supporting a short needle-shaped MW radiating antenna (Fig11, Fig 12).

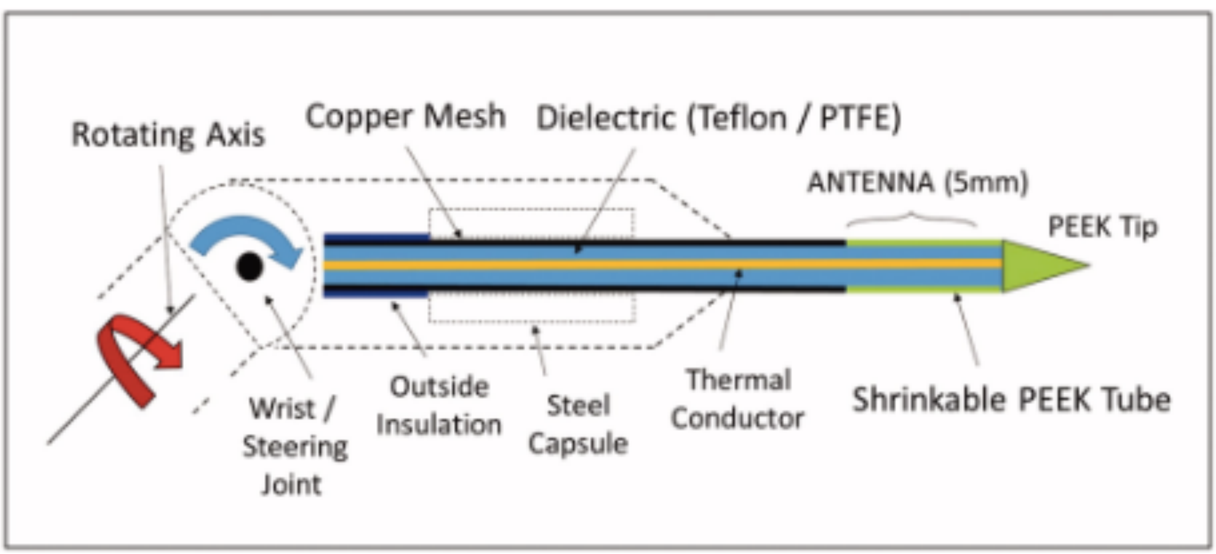

Fig 11. Schematic of the device

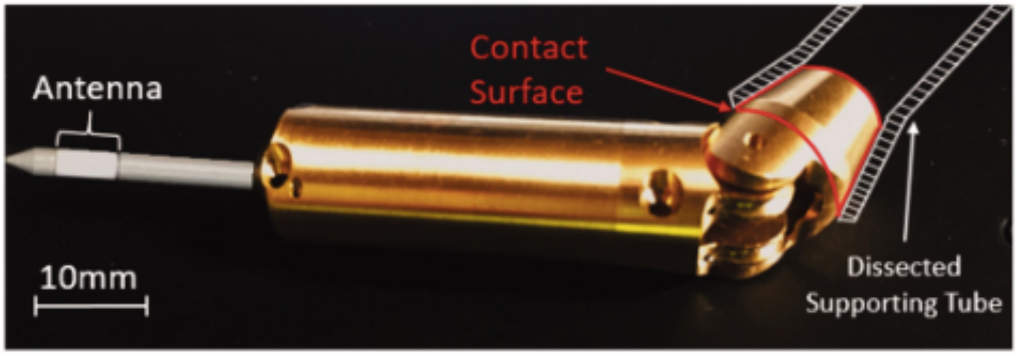

Fig 12. First real prototype in a bend state

Consequently the geometrical couplings and internal distribution of the components necessary for the functioning of the kinematics were designed to guarantee the maximum head steering angle of 120° (+60° up, −60° down), described as the optimum value by Adebar et al. [38]. This design had to guarantee an optimal intraoperative surgical maneuverability without introducing connection discontinuities and propagation losses between the feeding coaxial cable and radiating element (antenna). The main dimensional constraints of the device were in fact determined by its need to pass inside a standard laparoscopic trocar (12 mm). To improve the range of movement (ROM) of the device, a rotational degree of freedom (DOF) along the trocar's axis was included. This additional DOF was allowed by using two small radial ball bearings recessed on the internal stainless steel capsule (Fig 13).

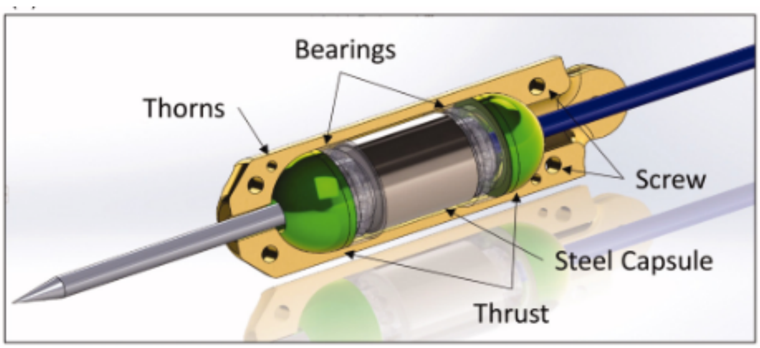

Fig 13. Internal mechanical structure

The device was connected to the MW generator by using a flexible coaxial cable with 2.1 mm external diameter, the axial sliding of which was prevented by the fixing in the steel capsule.

To eliminate the joint between the coaxial cable and radiating element, the needle was simply obtained as a straight extension of the coaxial feeding cable, drastically simplifying the whole structure and reducing possible causes of impedance mismatch. The end section of the needle, which must be inserted into the tissue, was coated with a thin layer of PEEK to increase its stiffness and robustness. PEEK is a biocompatible semicrystalline thermoplastic with excellent mechanical and chemical resistance properties that are retained at high temperatures. Electrical properties of the PEEK are: relative permittivity 3.5 , dissipation fact 1.5 x 10^ $^{-3}$. PEEK has a glass transition temperature of ~143 °C and melts at ~343 °C. We choose PEEK mainly because of its thermal resilience that permits multiple sequential insertions into the liver parenchyma without structural damage. Furthermore, the high mechanical flexibility of the feeding coaxial cable allows a wide angle for the steering of the device head, permitting it to reach different parts of the liver through the same trocar entrance.

Numerical Simulations

The numerical simulations were performed using two solvers. The objectives of the numerical simulations were to evaluate the effectiveness of the needle and the generator before starting to assembly the previously described device.

The first numerical simulation was conducted using the CST MICROWAVE STUDIO (https://www.cst.com) based on the finite element integration technique, which is a consistent discretization scheme for Maxwell's equations in their integral form.

The second part of the analysis was performed using Solidworks Flow Simulation (SFS) software (SolidWorks, Waltham Massachusetts, U.S.A.), which is a full 3D computation fluid dynamics (CFD) simulator capable of performing thermal analysis in fluids and solids considering conductive, convective, and irradiation exchange. This commercial solver on SFS is extremely flexible and works on the governing Navier–Stokes equation in its integral form with a discrete numerical technique based on the finite volume method. This method permits to analyze the flow behavior in internal cavities, such as vessels; in our specific case. The method considers the variation of the convection coefficient of the air surrounding the applicator. The air is treated as a free-flowing fluid, subject therefore to the effect of gravity. In fact, if heated, the fluid modifies its speed range by amplifying the convective exchange coefficient.

This choice was driven by the physical phenomena involved in the sequential ablation protocols: during the ablation pulse (Power ON) called the Power ON phase (ONph). The transient thermal analysis was performed using the CST Microwave Studio software, considering the simplifying hypothesis that electromagnetic (Maxwell) and thermal (Bio-Heat) equations are not coupled through the temperature dependence of the complex permittivity of the tissue. In the next phase (Power OFF), called Power OFF phase (OFFph), EM-radiated fields do not exist and the SFS permits concentration of computational resources based on the CFD analysis, considering with a higher flexibility in mesh refinement to more accurately analyze the geometrical complexity of the device. At the end of the ONph, we assumed a negligible delay time for extracting the needle from the ablated tissue and placing it in the next position. The transferred thermal field obtained from CST results defined the initial conditions for the OFFph on SFS.

Near the MW antenna, the evolution of tissue temperature due to a high pulsed energy is very difficult to predict owing to vaporization, carbonization phenomena, and tissue deformation. To reduce the numerical burden on the CST simulator, we assumed an analysis domain constituted by a time- and space-invariant homogeneous isotropic liver tissue. The boundary condition of a perfectly matched layer was applied to the border of the domain. Based on our consultation with the surgical team, we set the drilling (insertion) depth of the radiating antenna in the liver tissue at 18 mm.

Figure 14 shows the CST model used for the ONph simulation in which the wrist joint was eliminated to reduce the mechanical complexity.

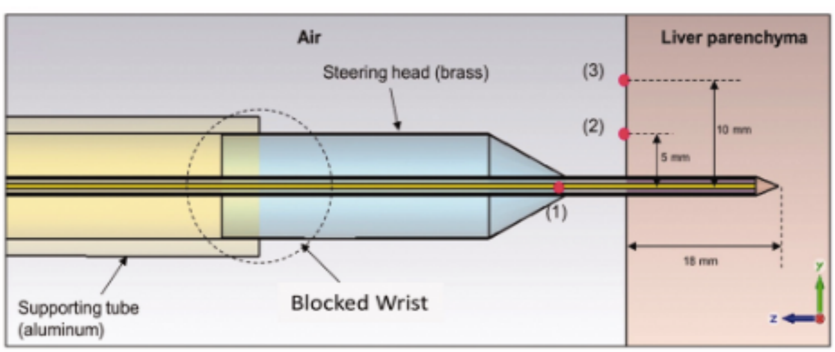

Fig 14. Computational domain configuration in CST

This simplified model allowed us to estimate the time-dependent temperature evolution both in the tissue and device head. For the subsequent comparison with the results of the experimental tests, point 2 and 3 (Fig 14) were taken as reference.

The SFS analysis domain is depicted in Figure 15. The geometrical heterogeneity was preserved and the mesh was refined according to the adaptive control of the solver that automatically identifies the most critical areas during computational calculation to reach the highest quality in terms of thermal distribution during the OFFph.

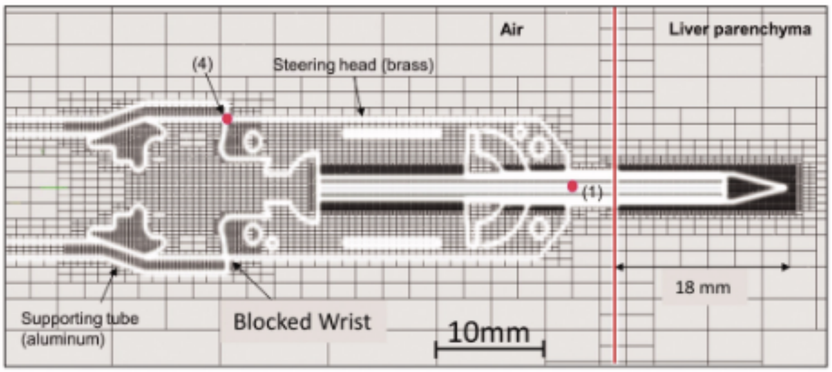

Fig15. Computational domain configuration in solidworks flow simulation (SFS): (1) internal temperature of input needle obtained through CST results; (4) output reference point for validation through thermocouple measurements.

The physical properties of the bovine liver, are listed in Table 1, and were used in both the simulation solvers.

Property	Value
Name	Liver
Density	1020 kg/m^3
Specific heat	3600 J/(kg*K)
Dielectric constant	53
Electrical conductivity	1.73 S/m
Thermal conductivity	0.469 W/(m*K)

Table 1: Physical properties of hepatic tissue at 2.45-GHz frequency

To reduce model complexity and computational time, the ball bearings were assumed as full steel cylinders; therefore, the numerical thermal results required experimental verification.

__Functional tests of MW generator and MW antenna__

The objectives of this tests were to confirm the previously described numerical simulations and to evaluate an optimal setting of the antenna and the generator that is able to produce a sufficient coagulation area in the shortest time. In this experimental setup we did not want to evaluate the joint movement but only the generator and antenna power so the experimental tests were conducted using the joint blocked in a straight position (Fig 16).

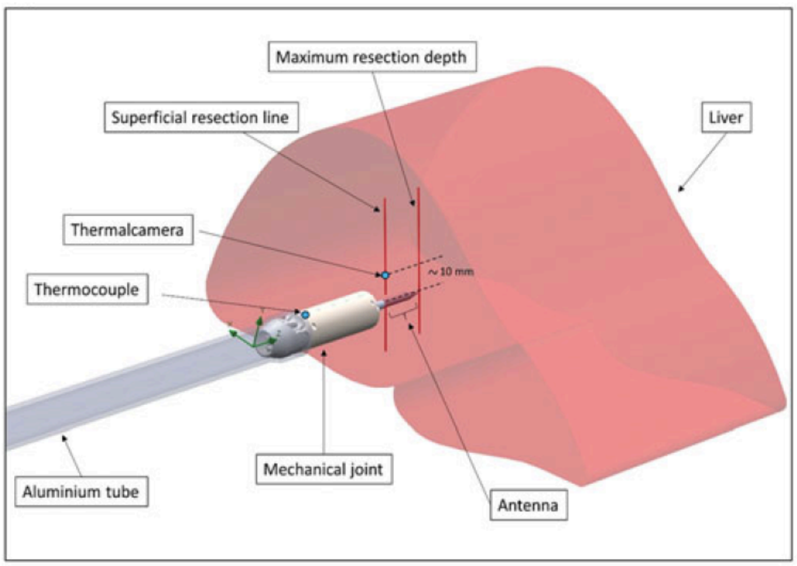

Figure 16. Schematic description of the proposed procedure.

An ex vivo bovine liver was used. The liver was transported to the lab in a portable cooler. The tissue was maintained at a temperature of 5 °C to prevent damage during transport, and then it was slowly brought back to room temperature of 20 °C before initiating the experiments. The tests were conducted at room temperature to obtain a series of thermally comparable test results. The input reflection coefficient of the antenna was continuously monitored to assure a matching better than −12 dB that corresponds to a reflected less than 10%. The procedures were tested using three protocols to determine which protocol produces the best ablation sizes while minimizing operating phase times and avoiding device overheating.

The Power OFF time, that is the time that elapses between an ablation and another, was set at 30 s and was not varied for each protocol, whereas Power ON time, that is the time when the needle is inserted into the liver parenchyma, was set at 20, 30, and 40 s, as show in Table 2. The MW generator was set at its maximum output power of 120 W. The insertion points of the needle into the liver were marked at liver capsule by the surgeon with a monopolar scalpel in order to predefine the ideal resection line for each liver lobe. Considering an theoretical ideal ablation of 1,5cm in diameter per each Power ON Time and willing to have some overlap between the ablations we set the predefined insertion point at 10mm distance each other along the pitch of the resection line. The angle of insertion was maintained perpendicular to the organ capsule and aligned with the gravity vector.

Table 2. Protocol duty cycle.

Protocol	On [s]	Off [s]
1°	20	30
2°	30	30
3°	40	30

Table 2: Protocol Duty Cycle

During all the experiments, we monitored the liver surface (capsule) temperature by using a thermal camera and the supporting aluminum-cylinder temperature by using a thermocouple (Figure 17). We tested the three simulated protocols separately, and measured ablation diameters at the end of each test. Finally, we tested the entire sequence of lobar hepatic resection comprising eight sequential ablations on predefined equidistant (10 mm) points.

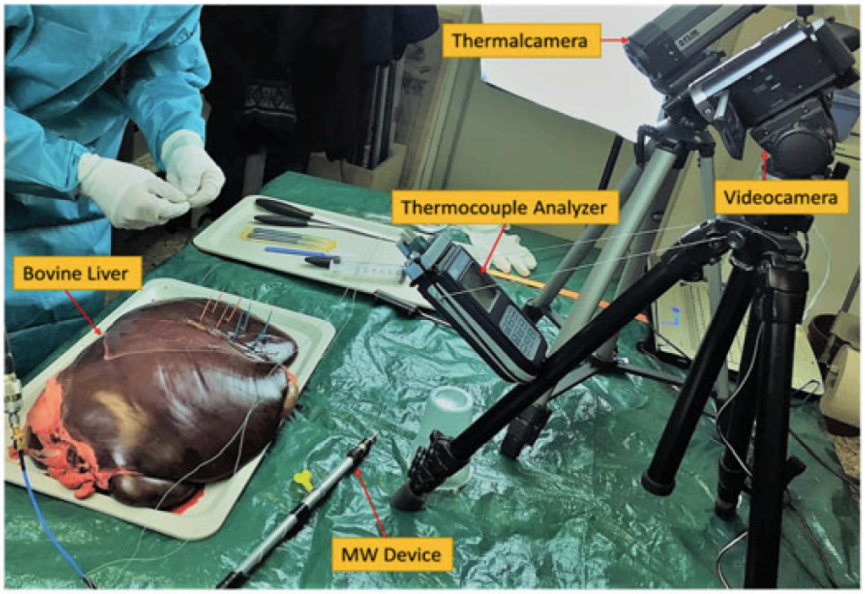

Fig17. Laboratory setup

Tool integration into the DvRK System

The new MW tool needed then to be integrated into a robotic arm of the dVRK surgical platform (Figure 18) both by hardware and software.

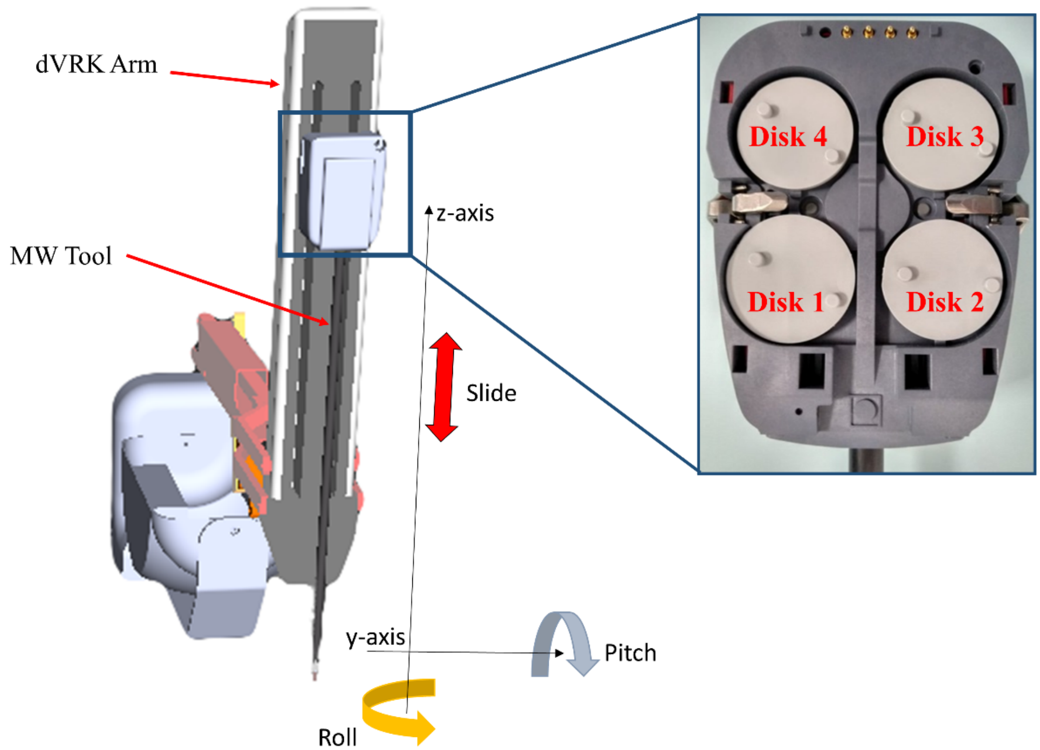

Figure 18. Scheme of the overall integration of the microwave tool in the dVRK robotic platform underlining the three allowed degrees of freedom (i.e., pitch, roll and slide). Inset: disks of the dVRK tool used to actuate the last four joints: roll; pitch; yaw and grip.

Hardware integration - The authors' efforts have been focused on the integration of the mechanical joint, equipped by the MW needle, as a tip of a traditional da Vinci tool. A permanent cautery spatula tool has been selected and disassembled. All steel cables and the tool tip have been removed, while only preserving the components used as interface between the tool and the robotic dVRK arm (hereinafter referred to as "tool head") and part of the carbon shaft. Thus, a new shaft for linking the joint to the tool head has been realized. The original shaft has been cut, keeping only the proximal segment to simplify the anchoring with the head tool, and it has been integrated with a steel tube 11.5 mm in diameter, suitable to pass through a 12 mm trocar, and 240 mm in length. The distal part of the shaft has been produced in metal material to guarantee a proper heat dissipation of the heat derived from the MW needle activation. The device temperature is reduced at a 0.4°C/s rate by natural convention with the ambient air when the MW generation is switched off [39]. Moreover, two braid polyethylene wires (Maciste, Mitsubishi Line, CHN), 0.26 mm in diameter with a payload of 14.7 kg, have been passed through the developed joint and fastened at one pulley of the tool head to enable the tool mechanical actuation. Figure 19 shows the realized tool and the main dimensions are reported. The tool is 550 mm in length whereas the tip is 85 mm long. Considering the design of the tool, the mechanical integration of the MW tool in the dVRK surgical robot has required minimal hardware modification: only a 12 mm trocar support has been realized and integrated into the dVRK arm, in order to firmly lodge the trocar and avoid any undesirable fluctuations of the tool shaft during the procedure. The additional support has been fabricated using a 3D printer machine (ProJet MJP 3600, 3D Systems, South Carolina, U.S.).

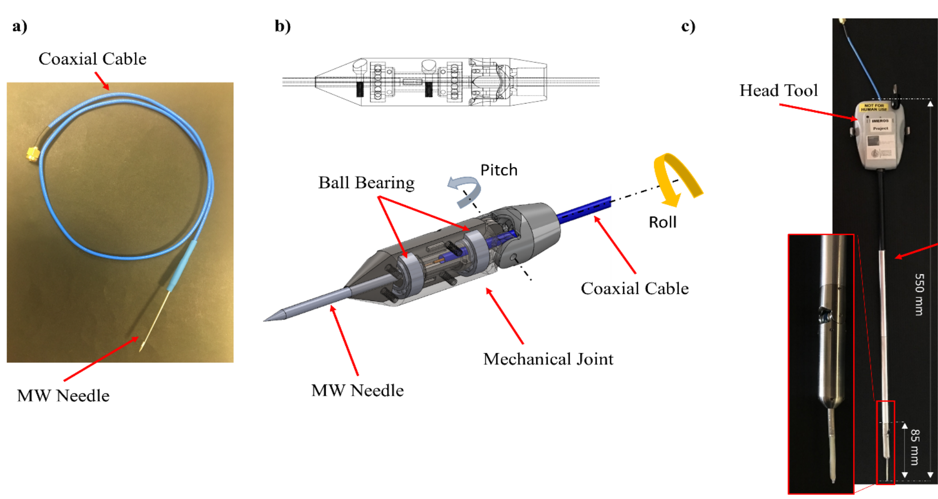

Figure 19. a) MW needle, b) CAD representation of the mechanical joint and c) final integrated tool.

Software integration -In this section, the implementation of the software part allowing a proper control of the MW tool is addressed. To this aim, it is important to introduce the different levels of the available open source software architecture used for teleoperating the dVRK, with reference to [40]. The required software modifications to the original platform in order to control the new tool in teleoperation are addressed in section II.b.

dVRK software architecture: For both master and slave arms of the dVRK (*i.e.,* two Master Tool Manipulators Left and Right (MTMR & MTML) and two Patient Side Manipulators (PSM1 & PSM2)), two software levels are used to ensure the whole teleoperation scenario: the low and the high level software.

The low level software is an intermediate layer between the high level algorithm running at the computer side and the hardware platform. It ensures the communication between the computer and the sensors and actuators of the dVRK robot. This level of software is composed of an embedded firmware at the FPGA/QLA boards and a C low level library (*i.e.,* AmpIO library). The algorithms running at the embedded firmware stage are ensuring: a) the collection of data from digital inputs and the control of digital outputs; b) the computation of encoder positions and velocities; c) the detection of overflow and preload; d) the performance of basic safety checks on motor current; e) the implementation of FireWire protocol to communicate with the computer; and f) to maintain a watchdog in order to guarantee the computer is communicating with the controllers. The second stage of the low level software part (*i.e.,* the C low level library code) runs on the computer side. It is in charge of the following tasks: packing/unpacking data to/from FPGA; handling multiple FPGAs and treating them as a single controller; testing the hardware part using simple programs.

The high level software, which includes interfaces to the Robot Operating System (ROS), consists mainly of a set of C++ threads running in parallel. This set of components is based on the cisst/SAW libraries, more specifically the cisstMultiTask framework. Different C++ classes are derived to manage the console, the teleoperation state machine, the PID controllers, and the arms kinematics computations. For the console classes, a configuration file (.json extension) is used in which the teleoperation structure is defined by the number of arms used and by the orientation of the slave arms with respect to the master ones. The arms classes use also configuration files in which the whole kinematic chain of each arm is described, including the Denavit Hartenberg (DH) parameters and the coupling between actuators and joints. In the next section, the configuration file of the new MW tool including its kinematics description is detailed.

dVRK Software modification: In the .json file of the dVRK slave arm, a section is dedicated to describe the mechanical coupling between the actuators variables $q \epsilon \mathbb{R}^7$ and the joints variables $\theta \epsilon \mathbb{R}^7$. The relation between actuators and joints variables is defined by a matrix, named coupling matrix $M \epsilon \mathbb{R}^{7 \times 7}$. For clarity, an example of the last four disks/joints coupling of the Large-Needle-Driver tool (*i.e.,* the standard tool of the dVRK) is shown in Figure 18.

The mechanical coupling between the last four joints (*i.e.,* roll, pitch, yaw, and grip) and the four actuated disks numbered from 1 to 4 are given by Table 3 which represents a (4x4) submatrix appearing in the coupling matrix M.

	Disk1	Disk2	Disk3	Disk4
Roll	-1.563	0.000	0.000	0.000
Pitch	0.000	1.018	0.000	0.000
Yaw	0.000	-0.830	0.608	0.608
Grip	0.000	0.000	-1.217	1.217

Table 3. The coupling between the disks of the dVRK tool and the last four joints: roll; pitch; yaw and grip.

As the mechanical chain of the new MW tool is different to the Large-Needle-Driver, the coupling matrix in the .json file should be adapted to fit with the new mechanical configuration. Even if only two disks are required to actuate the two last joints of the MW tool, which are the roll and the pitch, the other lines in the coupling matrix corresponding to the non-used joints should not be set to zero in the whole line in order to avoid singularity problems. Otherwise, deep modifications at the low level classes should be made, thus requiring more time and effort.

This condition is to keep the matrix M full rank and then invertible. The new coupling matrix respects this non-singularity condition and at the same time decouples the roll from the pitch as the disk 1 actuates only the roll and the disk 3 actuates only the pitch. This new decoupled configuration is different from the original one in which the actuation of only one disk from the three last ones contributes to the motion of two DoFs as shown in Table 3. The submatrix of the M matrix (M_{sb}) modified from the original configuration and which corresponds to the actuation of the four disks is given by:

$$M_{sb} = \begin{bmatrix} -1.563 & 0.000 & 0.000 & 0.000 \\ 0.000 & 0.000 & 0.250 & 0.000 \\ 0.000 & 1.000 & 0.000 & 0.000 \\ 0.000 & 0.000 & 0.000 & 1.000 \end{bmatrix}$$

The two remaining disks (*i.e.,* 2 and 4) are free *i.e.,* not connected mechanically to any joint, but their columns are not set to zero in order to respect the non-singularity condition (both are set to 1.000). They have no effect on the kinematics calculation, as the free disks are held at the software level during the teleoperation. The ratio disk1/roll is equal to the one corresponding to the Large-Needle-Tool (set to -1.563). It is obvious that the ratio 0.250 in the matrix M_{sb} corresponds to the gear ratio disk3/pitch. The coupling matrix M and its inverse are defined in the .json configuration file, which is used as an input by the arm classes to compute the kinematics. The jacobian matrix of the slave arm is obtained thanks to a solver class.

Another modification is required for the DH table included in the .json file of the Large-Needle-Driver. This DH table includes six mappings related respectively to the outer yaw; outer pitch; slide insertion; roll; pitch and yaw, without considering the grip (calculated separately and ignored in the case of the new MW tool). This modelling allows expressing the pose of the gripper base. For the new MW tool, only five mappings are required to express the pose of the needle base, these mappings are related respectively to the outer yaw; outer pitch; slide insertion; roll and pitch. The DH table parameters are adapted considering the new mechanical configuration of the tool attached to the slave arm. As the

DH table of the MW tool has one mapping less than the one of the Large-Needle-Driver, the last mapping related to the yaw joint in tool is changed by a linear constant translation with a quantity equal to the length of the last tool link. This modelling allows therefore expressing the pose of the distal extremity of the needle.

Assessment and validation: in-vitro, ex-vivo and in-vivo tests

The assessment of the MW tool has been demonstrated by means of in-vitro, ex-vivo and in-vivo experiments. For performing entire experimental sessions and considering that the dVRK version available at the authors' institute had no Endoscope Control Manipulator, two external cameras of type Logitech C270 have been integrated on the platform in front of the PSM arms and connected to the computer. The two images acquired from the cameras are displayed on the two screens of the dVRK High Resolution Stereo Viewer (HRSV) through a multi-display Matrox graphics card.

The hardware and software validation has started with in-vitro tests to evaluate the intuitiveness, robustness and reliability of the system. The developed tool has been fixed on one dVRK arm, passing through a 12 mm trocar, and different motions have been performed. These preliminary results have been used for the final optimization of the realized tool; then, ex-vivo tests have been carried out to prove the effectiveness of the proposed device in a real scenario.

The experimental scenario has been purposely prepared: the tool has been integrated on the right arm of the surgical robotic platform and a freshly excised porcine liver (weight about 650 g) has been arranged on the table under the robotic arms. The left-robotic arm has been equipped with a Prograsp Forceps (Intuitive Surgical Inc, Sunnyvale, CA), a traditional tool used for tissues and organs manipulation. We performed a liver resection using the developed MW tool mounted on the right arm; the test protocol has been the following:

- The tool was placed on the right-robotic arm of the dVRK;
- The tool passed through the trocar and the target area was reached;
- The surgeon manipulated the robotic arms (*i.e.,* the right arm equipped with the MW tool and the left arm with a forceps) as when performing the hepatectomy using coagulative necrosis aided resection;
- The tool needle was inserted by the surgeon along the predefined resection line using the dVRK robotic platform;
- The tool was then turned on with 120 W power for 30 s and subsequently extracted and reinserted 10 mm away from the previous insertion point along the ideal resection line;
- The procedure was then repeated until all the insertion tasks are concluded and the precoagulation of the resection line was completed.

During the validation test, a thermal image camera (ThermoVision, Flir Systems, Oregon, U.S.) has been used to collect the heat distribution on the tool and the external surface of the excised liver. Moreover, in order to analyse the smoothness of surgeon gesture and of the MW tool in teleoperation, a Python application has been developed and integrated into the software platform. This application allows for the acquisition and the storage of the data needed (*i.e.,* Cartesian positions and velocities) by subscribing to the ROS topics publishing these data in real time.

Finally, an in-vivo test has been performed with the surgical team using one pig model(*i.e.,* male pig, 45 kg) in accordance with Italian animal protection law provisions, approved by the ethics regional committee. The experimental session has been carried out under the guidance of qualified veterinary and a surgeon for validating the coagulative efficacy of the developed tool in a perfused in-vivo liver model. We decided not to use the dVRK robotic platform in-toto for the in-vivo experimentation because the surgical robot is a bulky and cumbersome platform that is difficult to assembly and integrate in the animal setting. Moreover, the aim of the in-vivo test session was only to validate the coagulative effect of the developed tool considering that its dexterity and manoeuvrability have been evaluated during the previously described in-vitro and ex-vivo test sessions. Thus, the efficacy of the MW tool has been proved using the developed device without the robotic platform.

The complete surgical test procedure has involved the following steps:

- The surgeons performed a bilateral subcostal incision and reached the liver;
- Right and left triangular ligaments, falciform ligament and coronary ligament were resected to allow a complete liver mobilization;
- The Glisson's capsule was marked using a monopolar eletrocautery and a resection line was outlined with the needle insertion points set at 10 mm apart;
- The MW needle was inserted in the target point and the generator was is turned on with 120 W power for 30 s and subsequently extracted for 20 s waiting. The procedure was then repeated for all the predefined target points;
- At the end of the procedure the surgeon performed a cold scalpel transection of the liver lobe along the previously coagulated resection line;
- The liver bleeding was evaluated using a visual scale ranging from 0 to 5 (*i.e.,* 0=perfect haemostasis, 5=completely ineffective haemostasis);
- A definitive haemostasis was obtained with surgical stiches if necessary;
- This procedure was repeated for each liver lobe (i.e., four times);
- According to the study protocol, the pig was euthanized by the veterinary after the experiment.

- In this way, a multiple open MW assisted liver lobectomy was performed.

RESULTS

CST Simulations Results

Figure 20 shows the Power ON phase results on the three references points (Point1-Point2-Point3) obtained through CST analysis.

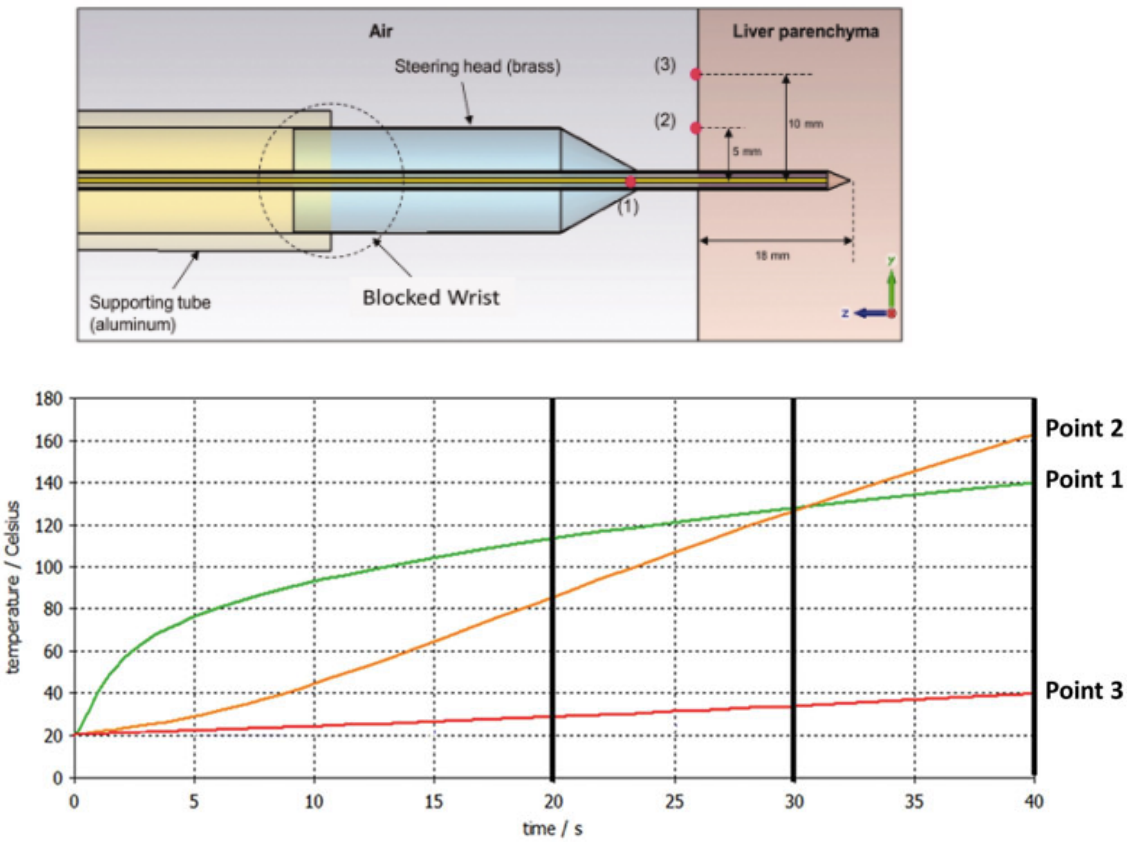

Temperature	t = 20 s	t = 30 s	t = 40 s
Point 1 (Needle)	113 °C	128 °C	138 °C
Point 2 (5 mm)	86 °C	126 °C	163 °C
Point 3 (10 mm)	29 °C	33.8 °C	39.8 °C

Figure 20: Temperature evolution results obtained using the CST simulator

It is worth noting that the probe at point 1 is subject to more heat sink effect caused by conduction as it is in direct contact with the metal part. In contrast, point 2, being closer to the antenna and not in direct contact with the metal armor, dissipates heat only because of the effect of convection with the air on the surface of the parenchyma, thus resulting in higher temperatures at the end of the procedures.

At the end of Hot Phase, we collected the corresponding ablation diameters on the liver surface, considering the region of tissue enveloped by the 60-°C isothermal curve (blue), as shown in Figure 21. This threshold was selected to match a secure coagulative necrosis temperature.

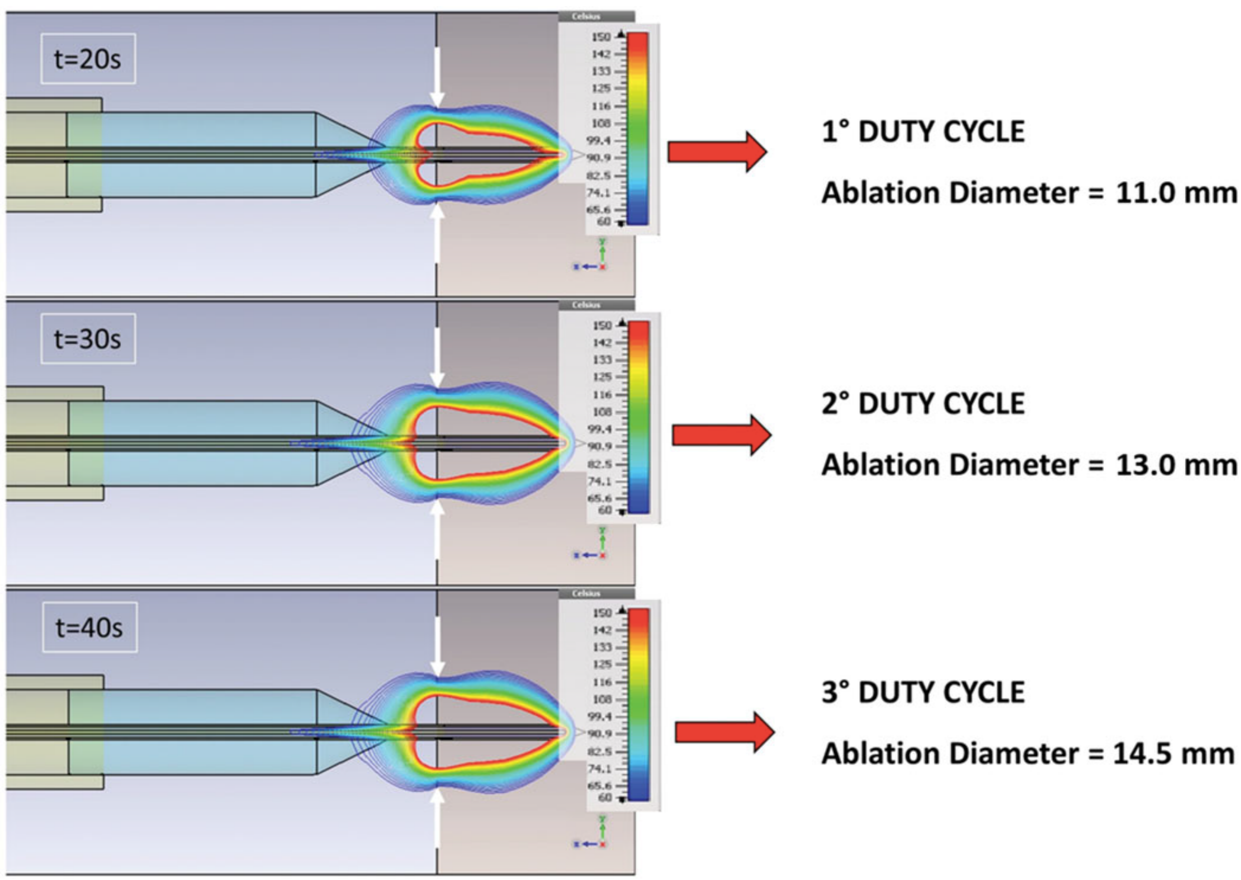

Figure 21. Isothermal distributions on the Y–Z plane of the protocol-coupled thermal EM simulations

SFS Simulations Results

The ONph behavior at the end of the CST simulation was assumed as the initial condition for SFS OFFph simulation. By using the SFS software, we obtained the OFFph temperature evolution shown in Figures 22 and 23 at points 1 and 4, respectively.

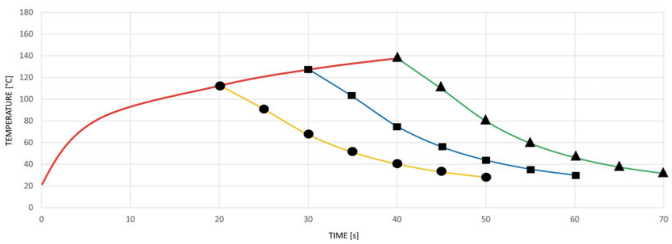

Time	t = 20 s	t = 30 s	t = 40 s	t = 50 s	t = 60 s	t = 70 s
1° PROTOCOL	113°C	67°C	40°C	28°C		
2° PROTOCOL	113°C	128°C	75°C	43°C	30°C	
3° PROTOCOL	113°C	128°C	138°C	79°C	46°C	32°C

Figure 22. Temperature evolution at Point 1 for different protocols (ONph: red boxes, OFFph: blue boxes)

The red curve in Figure 22 represents the thermal data captured during the ONph by using the CST simulator. As expected, the needle temperature rapidly decreased because its thermal inertia was very low. The aluminum cylinder, with higher thermal inertia, showed a gradual increase in temperature during the application of all the protocols.

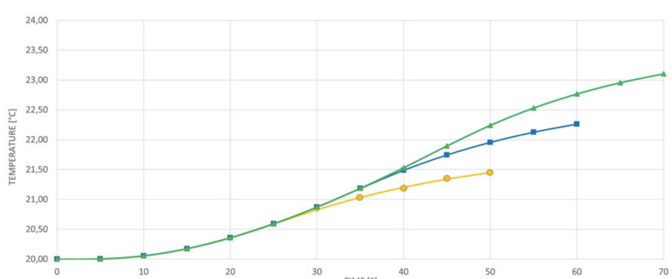

Time	t = 20 s	t = 30 s	t = 40 s	t = 50 s	t = 60 s	t = 70 s
1° PROTOCOL	20.36°C	20.83°C	21.20°C	21.45°C		
2° PROTOCOL	20.36°C	20.87°C	21.49°C	21.96°C	22.26°C	
3° PROTOCOL	20.36°C	20.87°C	21.53°C	22.24°C	22.77°C	23.10°C

Figure 23. Temperature evolution at Point 4 for different protocols (HPh: red boxes, CPh: blue boxes)

At the end of the OFFph, the thermal field showed a symmetrical polar distribution around the *Z* axis. Figure 24 shows the thermal behavior results for the three simulated protocols, highlighting the maximum temperature and temperature gradient at point 4.

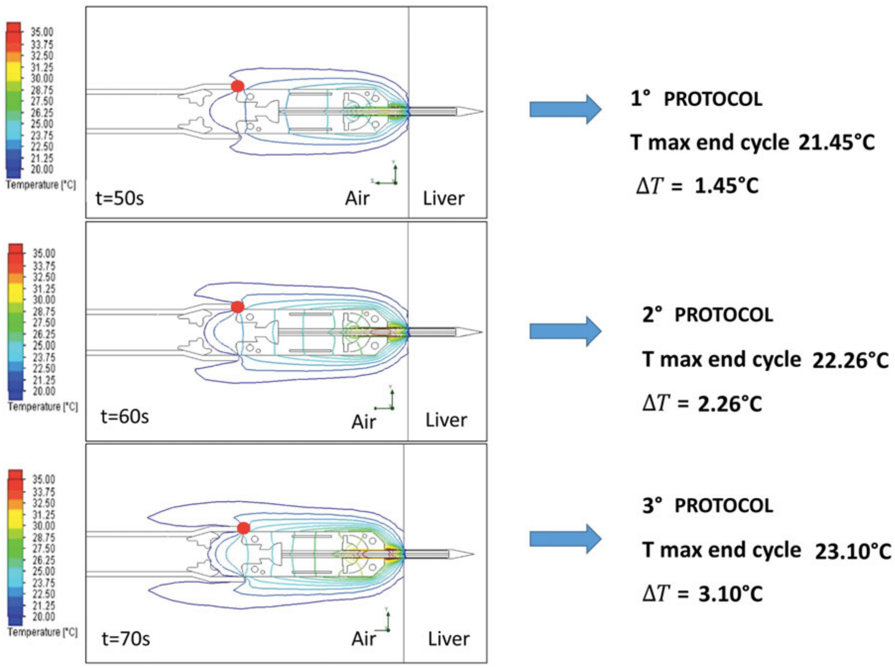

Figure 24. Isothermal distributions on the Y–Z plane of the thermal field on SFS

Ex vivo test results

As a result of localized overheating, uncooled applicators showed limitations for the continuous power supply. In this study, the metallic mass of the device worked as an efficient heat sink and thermal stabilizer, increasing the durability and resilience of the applicator even at high power levels.

By using the newly developed device, we performed 120 ablations without any apparent degradation and input impedance mismatch. Single ablation procedures by using the three protocols were repeated eight times (total n = 24), and eight sequential ablations were repeated four times (total n = 96).

The superficial ablation diameters for single and sequential procedures were almost the same because they essentially depend on the energy transferred to the tissue during the power-on phase of each protocol. For the first protocol (2.4 KJ pulse), the mean diameter was 9.2 mm with a variance of 0.22 mm; for the second protocol (3.6 KJ pulse), the mean diameter was 12.7 mm with a variance of 0.35 mm; and for the third protocol (4.8 KJ pulse), the mean diameter was 14.6 mm with a variance of 0.58 mm (Figure 25(a)). The diameters were also confirmed by matching the measurements of the 60°C isothermal line on the thermal camera images (Figure 25b).

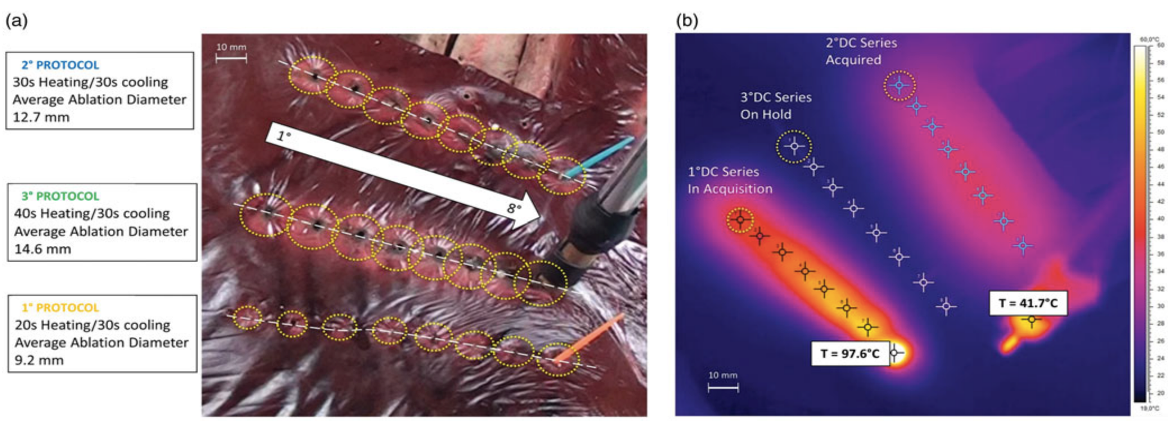

Figure 25. Protocols ablation series: a) difference in the superficial radius dimensions in each protocol; b) Thermal image at the end of eight sequential ablations using the 1°-protocol

After each sequential ablation procedure, the liver was cut along the predefined resection line to assess measurements and quality of ablation. For the 1°, 2° and 3° protocols, we measured coagulated areas of approximately 90 mm × 25 mm, 100 mm × 30 mm, and 105 mm × 33 mm, respectively.

As a first gross assessment, the surgeon evaluated the quality of the coagulated area. The resection line was free of tissue charring and carbonization, and presented the best homogeneous area of well coagulated tissue with 2° protocol application (Figure 26).

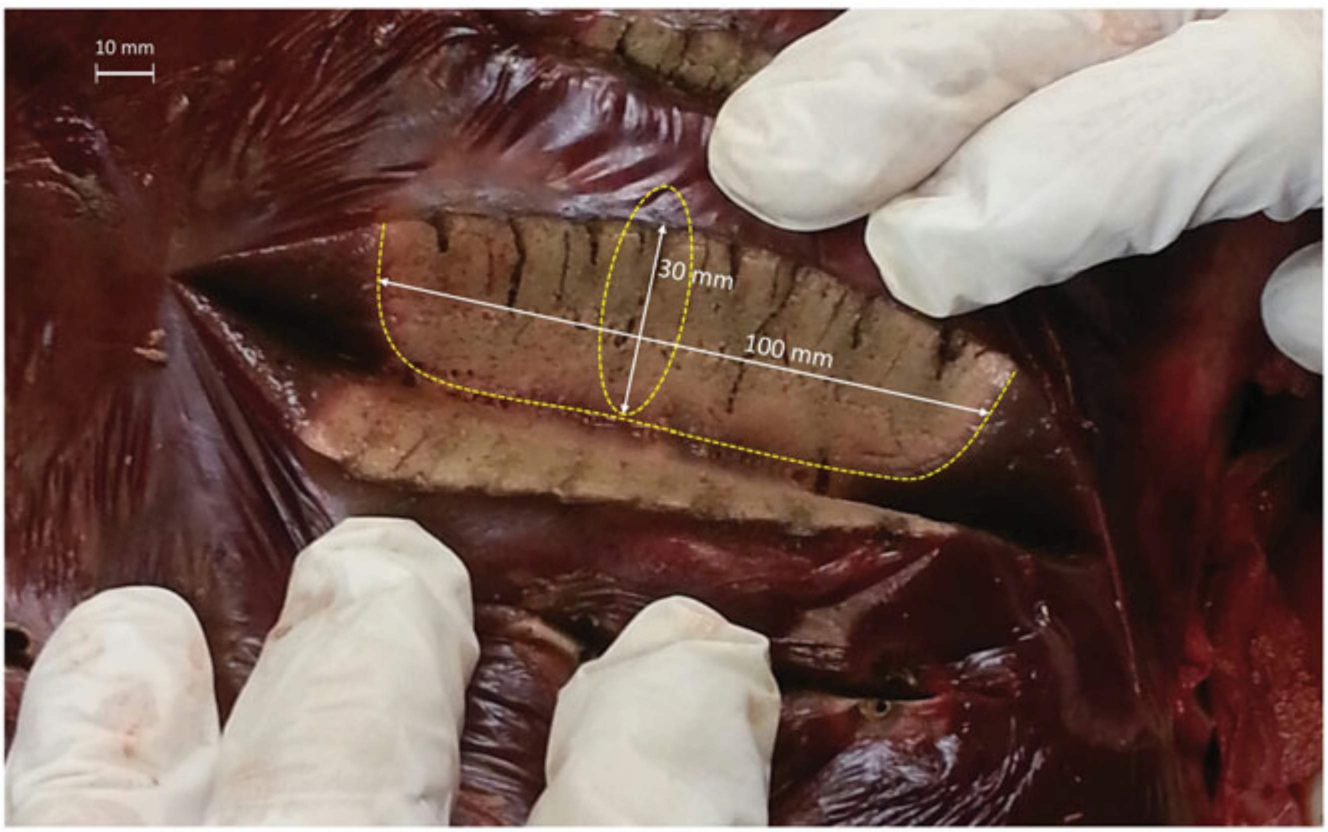

Figure 26. Coagulated area after eight ablations: dimensional references refer to the 2° protocol

Temperature measurements acquired through the thermal camera were collected for each protocol on single and sequential ablations to validate CST simulations. The temperature was measured at points 2 and 3 (See Fig. 20). During the application of the first, second, and third protocols, the temperature ranges at point 2 were 20–125, 20–

150, and 20–161 °C, respectively. During the application of the first, second, and third protocols, the temperature ranges at point 3 were 20–30, 20–34, and 20–37.8 °C, respectively. However, the maximum temperature varied for different protocols, and the temperature gradient measured at points 2 and 3 was the same for all the protocols (Figure 27).

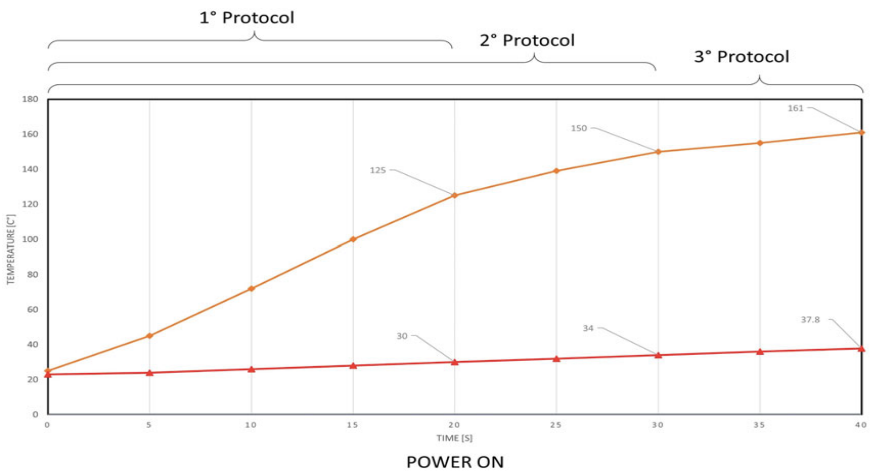

Figure 27. Mean statistical temperature evolution measured using the thermal camera: orange and red curves represent temperature evolution at Points 2 and 3, respectively

Figure 28 shows the average temperature evolution measured using the thermocouple at point 4 (See Fig. 15) for different protocols.

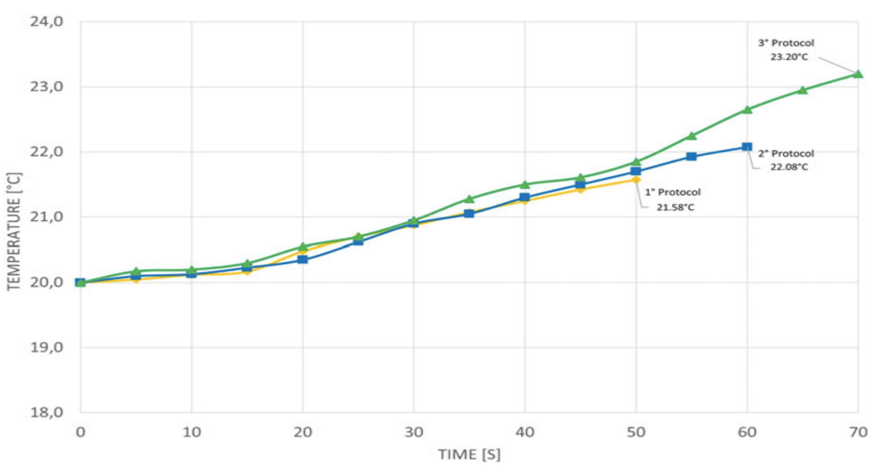

Figure 28. Average temperature evolution measured using the thermocouple: the yellow, blue, and green lines represent the temperature evolution for 1°, 2°, and 3° protocols

Integration on DvRK Results

The integration of the developed MW tool on the dVRK robotic platform has been successfully achieved, both at the hardware and software level. Figure 29 shows the final result where the MW tool has been lodged on the left arm (called PSM 1) of the robot. The tool passes throughout a traditional 12-mm trocar fixed by an ad hoc developed support. The MW tool exploits the DoF of the robotic arm (*i.e.,* outer yaw and outer pitch) and it guarantees three DoF (*i.e.,* pitch, roll and slide).

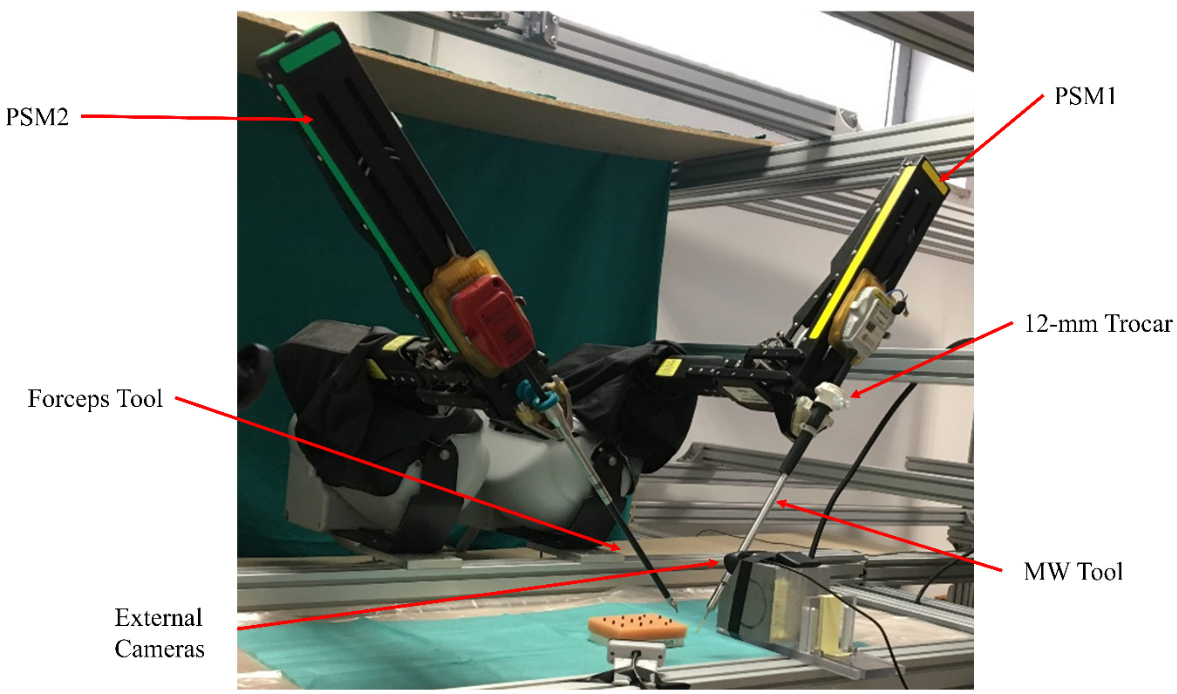

Figure 29. MW tool integration on dVRK robotic platform.

During ex-vivo experiments (Figure 30a), the MW tool was teleoperated from the surgical console through the master arm relying on the integrated vision system for the visual feedback. The positioning and the orientation of the MW needle during the insertion in the liver have been successfully performed for 50 times with 30 sec. power ON, subsequent

30 sec. of power OFF and about two seconds for each repositioning. The complete test was completed in about 51minutes.

a) b)

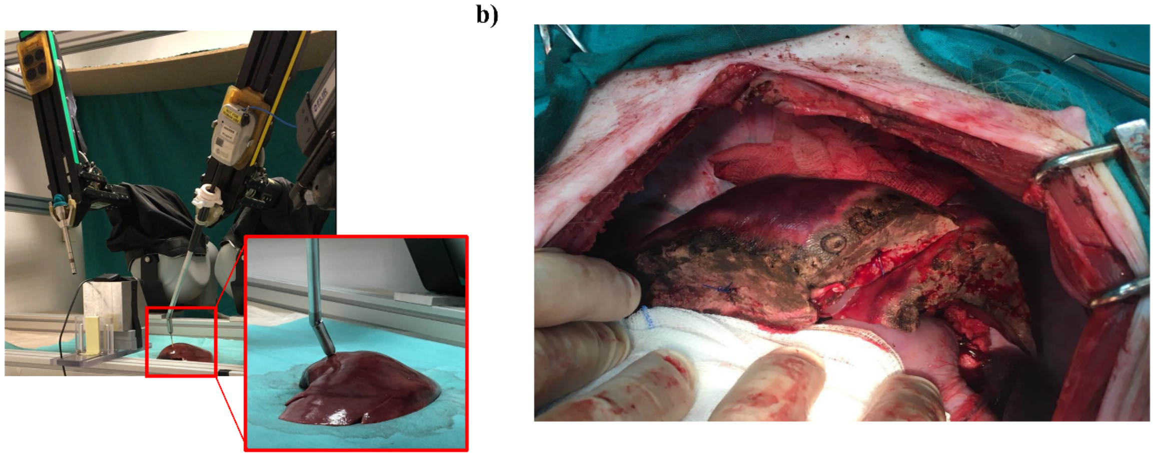

Figure 30. a) Ex-vivo and b) in-vivo test sessions.

For the entire test, the 3D Cartesian position and the orientation joints (*i.e.,* roll and pitch) was controlled in order to reach the liver surface and then to insert the MW needle inside the liver for the coagulation process. A scaling factor of 1/5 between the master arm motion manipulated by the surgeon and the slave arm supporting the new MW tool was used for improving precision during the teleoperation phase. Once the hand motion of the surgeon manipulating the master arm reaches the extremity of the workspace, the clutch pedal was used for repositioning the master arm. The slave arm was held when the clutch pedal is pressed and, once the clutch is released, the slave arm was teleoperated following the master arm motion (each arm in its own frame). A total of fifty sequential ablations have been performed on the explanted liver using the MW tool powered at 120 W for 30 s. Analysing the thermo-camera data, the air-liver interface temperature has never reached 50° C in accordance with the results of the previously described numerical simulations.

Figure 31 shows both master and slave end effector motions during the positioning and insertion of the MW needle inside the liver. The part of the operation reported here is between two presses of the clutch pedal *i.e.,* without discontinuity of the motion.

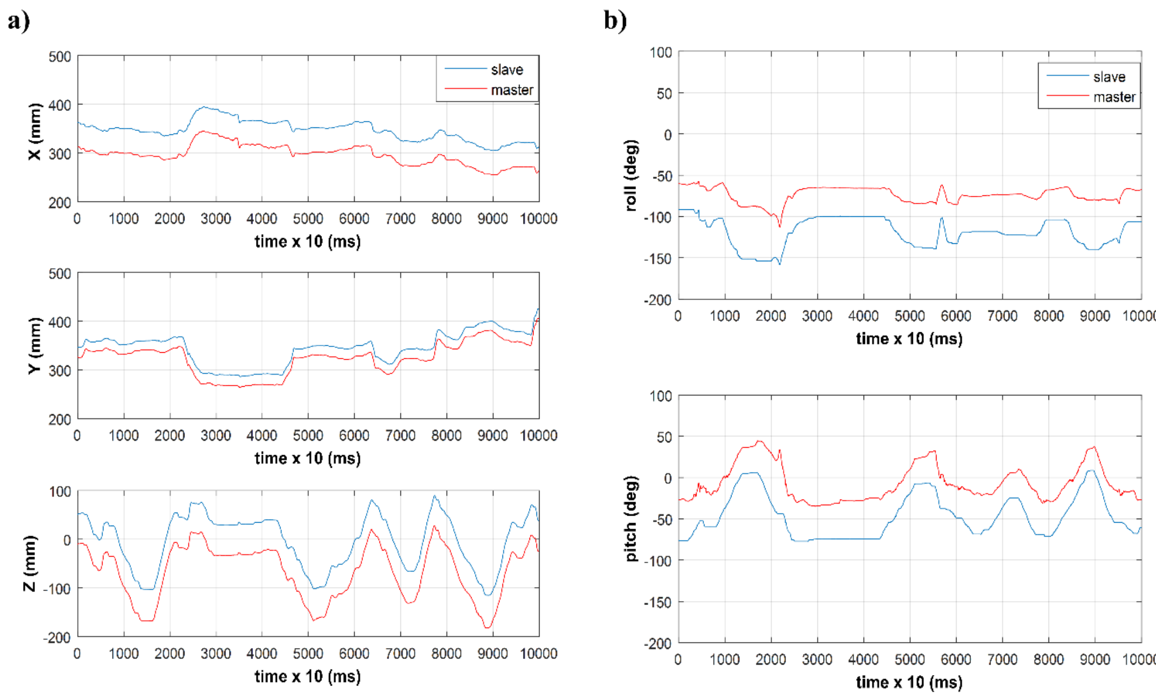

Figure 31. a) 3D motions and b) rotation (i.e., roll and pitch) of PSM and MTM tip

In Figure 31a, the 3D Cartesian positions of both master and slave are shown: the hand motion of the surgeon is smooth and the slave is perfectly following the motion of the master with a shift at the three position components due to the first press of the clutch for repositioning the master arm. The highest amplitude of the motion is along the Z axis, which corresponds to the insertion axis. Two other DoF are added to the MW tool: the roll and the pitch which are controlled during the insertion of the MW needle; motions of these joints for both master and slave are shown in Figure 31b. In general, both pitch and roll are correctly teleoperated, except some cases in which they were slightly affected by the interaction force of the MW needle during the insertion inside the liver. This effect is not very pronounced as it can be seen from the curves of both roll and pitch of the MW tool which are following correctly their corresponding master roll and pitch joints. It is worth explaining that the shift between the master and the slave curves in Figure 31b is due to the shift in cabling between the roll/pitch joints and the PSM disks. This shift is corrected at the .json configuration file of the PSM arm by a readjustment: thus, the procedure of teleoperation is not affected by this shift. The master/slave scaling factor has been taken into consideration in Figure 31 for an evaluation at the same scale.

Finally, the animal test session (Figure 30b) confirmed the ablation potential of the MW tool also in a real setting. The results have been summarized in Table 4 where, for each lobe, the number of the ablation needed for the liver lobe resection, the resection sizes in terms of length, width and thickness, the bleeding visual index and the actions performed after the MW tool application are reported. We performed four lobectomies using one pig. 30 ablations have been carried out with 120 W for 30 sec power on and 30 sec power off, following the protocol described previously. For each lobe, we needed a mean of 8 ablations (ranging from 6 to 10) to complete the respective procedure depending on liver lobe dimensions. The resection of each liver lobe was completed in about 10minutes depending on the length of the resection line and the liver lobe dimension. The length of the ablated tissue along the pre-marked resection line ranged from 60 to 75 mm (mean 69 mm). The width of the ablated tissue ranged from 10 to 25 mm (mean 16 mm). The thickness of the ablated tissue ranged from 20 to 45 mm (mean 32 mm). The evaluation of the obtained haemostasis ranged from 1 to 2.5 (mean 1.6). For one MW assisted lobectomy (*i.e.,* test number 2 reported in Table 4), we completed the resection without any other haemostatic procedures. In the other three resections, the haemostasis has been finalized with a haemostatic stich over a vessel with the diameter up to 4 mm. Complete hemostasis has been always obtained for vessels up to 4 mm in diameter.

Test	***Ablations number***	***Sizes (length, width, thickness) [mm]***	***Bleeding index***	***Post MW haemostasis action***
1	7	70 x 10 x 20	2.5	4 mm vessel stitched
2	6	70 x 15 x 35	2	-
3	10	60 x 15 x 30	1	8 mm vessel stitched
4	7	75 x 25 x 45	1	5 mm vessel stitched

Table 4. Details of the each lobe liver resection in terms of number of ablation, size of the resection area, bleeding index and post MW haemostasis action.

Figure 32 shows the bloodless margin of three liver lobes after MW precoagulation of the resection line and subsequent cold scalpel transection.

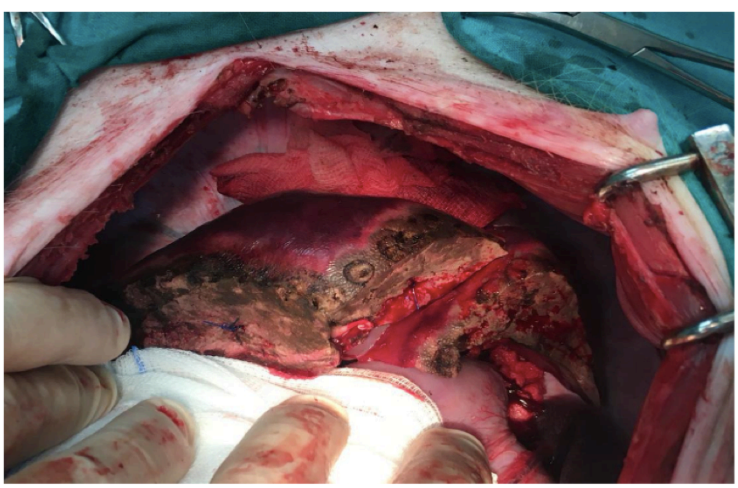

Figure 32

CONCLUSIONS

One of the main reasons of the slow spreading of robotic hepatic surgery is probably due to the difficulty to have a secure haemostasis during hepatic transection. Although the improvement of surgical techniques and instruments, bleeding from parenchyma transection remains one of the most critical point which importantly affects post-operative recovery. We demonstrated that numerical electromagnetic and thermal simulations are effective in developing a MWA device optimized for laparoscopic and robotic procedures and that the newly developed MW device joins the advantages of MW energy as a coagulative energy source with the advantages of robotics in minimally invasive surgery procedures.

To the best of the authors' knowledge, this is the first time that a MW tool has been developed and integrated into a cable-driven teleoperated surgical robot (*i.e.,* dVRK robotic platform). Thanks to the software integration, the MW tool can be seamlessly integrated in the dVRK (so that derived tools could be directly interfaced with the da Vinci system). Therefore, the teleoperation of the MW tool resulted intuitive for surgeons with previous robotic surgery experience. On the other hand, due to the hardware integration, the developed tool can be easily lodged in the robotic platform, thus possibly exchanged as needed, without additional efforts by the users. The MW tool has dimensions compatible with laparoscopic and robotic interventions because it can be easily inserted into a traditional laparoscopic 12 mm-trocar.

Both the in-vitro and ex-vivo test sessions and the surgeons experience confirms the potentiality and the user friendly of the developed tool. With the limitations of a small number of in-vivo procedures, the proposed tool seems to be very effective to reach complete liver coagulation necrosis along the pre-marked resection line. The tool achieves complete coagulative necrosis of liver parenchyma in only 30 seconds. A major advantage of this technique is the minimal lateral spreading of MW, thus avoiding to damage the surrounding tissue. A mean of 15 mm width of coagulated tissue is sufficient to guarantee a definitive haemostasis of vessels up to 4 mm in diameter even after adrenalin induced hypertension ensuring a minimal healthy liver tissue damage. Macroscopic bile leak was not encountered.

The MW tool has the potential to carry out a hepatic resection ensuring effective operation, organ/tissue safety, and preventing iatrogenic internal damage during surgery because it combines a powerful energy in an integrated cable driven robotic instrument. If further developed, this tool could extend the MIS procedures about the liver resection with zero blood loss and minimal use of sutures, surgical knots, clips or glue. During operation, more effective and easier bleeding control may encourage surgeons to perform more minimally invasive liver resections, thus extending to more patients the advantages of MIS.

REFERENCES

1- Lieto E, Galizia G, Cardella F, Mabilia A, Basile N, Castellano P, Orditura M, Auricchio A.
Indocyanine Green Fluorescence Imaging-Guided Surgery in Primary and Metastatic Liver Tumors.
Surg Innov. 2018 Feb;25(1):62-68.

2-Available: http://iarc.fr

3- Ayav A, Jiao LR, Habib NA.C Bloodless liver resection using radiofrequency energy. Dig Surg. 2007;24(4):314-7

4-Aldrighetti L, Pulitanò C, Arru M, Catena M, Finazzi R, Ferla G. "Technological" approach versus clamp crushing technique for hepatic parenchymal transection: a comparative study. J Gastrointest Surg. 2006 Jul-Aug;10(7):974-9.

5- Forner A, Reig M, Bruix J. Hepatocellular carcinoma.
Lancet. 2018 Mar 31;391(10127):1301-1314.

6- Romano F, Garancini M, Uggeri F, Degrate L, Nespoli L, Gianotti L, Nespoli A, Uggeri F. Bleeding in Hepatic Surgery: Sorting through Methods to Prevent It. HPB Surg. 2012;2012:169351.

7- Feng Q, Chi Y, Liu Y, Zhang L, Liu Q. Efficacy and safety of percutaneous radiofrequency ablation versus surgical resection for small hepatocellular carcinoma: a meta-analysis of 23 studies.
J Cancer Res Clin Oncol. 2015 Jan;141(1):1-9.

8- Xiao WK, Chen D, Hu AB, Peng BG, Guo YZ, Fu SJ, Liang LJ, Li SQ.
Radiofrequency-assisted versus clamp-crush liver resection: a systematic review and meta-analysis.
J Surg Res. 2014 Apr;187(2):471-83.

9- Qi X, Tang Y, An D, Bai M, Shi X, Wang J, Han G, Fan D.
Radiofrequency ablation versus hepatic resection for small hepatocellular carcinoma: a meta-analysis of randomized controlled trials.
J Clin Gastroenterol. 2014 May-Jun;48(5):450-7.

10- Sasaki K, Matsuda M, Hashimoto M, Watanabe G.
Liver resection for hepatocellular carcinoma using a microwave tissue coagulator: Experience of 1118 cases.
World J Gastroenterol. 2015 Sep 28;21(36):10400-8.

11- Curro G, Bartolotta M, Barbera A, Jiao L, Habib N, Navarra G.
Ultrasound-guided radiofrequency-assisted segmental liver resection: a new technique.
Ann Surg. 2009 Aug;250(2):229-33.

12- Sasaki K, Matsuda M, Hashimoto M, Watanabe G.
Liver resection for hepatocellular carcinoma using a microwave tissue coagulator: Experience of 1118 cases.
World J Gastroenterol. 2015 Sep 28;21(36):10400-8.

13- Zhou XD, Tang ZY, Yu YQ, Ma ZC, Xu DB, Zheng YX, Zhang BH.
Microwave surgery in the treatment of hepatocellular carcinoma.
Semin Surg Oncol. 1993 Jul-Aug;9(4):318-22.

14- Tabuse K, Katsumi M, Kobayashi Y, Noguchi H, Egawa H, Aoyama O, Kim H, Nagai Y, Yamaue H, Mori K, et al.
Microwave surgery: hepatectomy using a microwave tissue coagulator.
World J Surg. 1985 Feb;9(1):136-43.

15- Brace CL.
Microwave tissue ablation: biophysics, technology, and applications.
Crit Rev Biomed Eng. 2010;38(1):65-78.

16- Zhang M, Ma H, Zhang J, He L, Ye X, Li X.
Comparison of microwave ablation and hepatic resection for hepatocellular carcinoma: a meta-analysis.
Onco Targets Ther. 2017 Oct 3;10:4829-4839.

17- Biffi Gentili G, Ignesti C.
Dual applicator thermal ablation at 2.45 GHz: a numerical comparison and experiments on synchronous versus asynchronous and switched-mode feeding.
Int J Hyperthermia. 2015;31(5):528-37.

18- Berber E, Akyildiz HY, Aucejo F, Gunasekaran G, Chalikonda S, Fung J.
Robotic versus laparoscopic resection of liver tumours.
HPB (Oxford). 2010 Oct;12(8):583-6.

19- Korean Liver Cancer Study Group (KLCSG); National Cancer Center, Korea (NCC).
2014 KLCSG-NCC Korea Practice Guideline for the Management of Hepatocellular Carcinoma.
Gut Liver. 2015 May 23;9(3):267-317.

20- Vitiello V, Lee SL, Cundy TP, Yang GZ.
Emerging robotic platforms for minimally invasive surgery.
IEEE Rev Biomed Eng. 2013;6:111-26.

21- Lanfranco AR, Castellanos AE, Desai JP, Meyers WC.
Robotic surgery: a current perspective.
Ann Surg. 2004 Jan;239(1):14-21.

22- Diana M, Marescaux J.
Robotic surgery.
Br J Surg. 2015 Jan;102(2):e15-28.

23- Available: https://www.intuitive.com/

24-P. Kazanzides, Z. Chen,A. Deguet, G.S. Fischer, R. H. Taylor, and S. P. DiMaio
"An open-source research kit for the da Vinci® Surgical System," in *Robotics and Automation (ICRA)*
2014 IEEE International Conference on, 2014, pp. 6434-6439

25- J. Xu, Z. Song, and Z. Jia
"A robotic surgery navigation system for hepatic microwave coagulation therapy," in *Automation and Logistics, 2009.*
ICAL'09. IEEE International Conference on, 2009, pp. 1911-1916

26- Xu J, Jia ZZ, Song ZJ, Yang XD, Chen K, Liang P.
Three-dimensional ultrasound image-guided robotic system for accurate microwave coagulation of malignant liver tumours.
Int J Med Robot. 2010 Sep;6(3):256-68.

27- Liu S, Xia Z, Liu J, Xu J, Ren H, Lu T, Yang X.
Liver Tumor Therapy.
PLoS One. 2016 Mar 16;11(3):e0149482.

28- S. Morikawa, S. Naka, H. Shiomi, H. Murayama, K. Murakami, T. Tani*, et al.*,
Development of instruments to assist accurate puncture of liver tumors for MRI-guided microwave ablation
Journal of Microwave Surgery, 2012vol. 30, 183-190.

29- Morikawa S, Inubushi T, Kurumi Y, Naka S, Sato K, Tani T, Yamamoto I, Fujimura M.
MR-guided microwave thermocoagulation therapy of liver tumors: initial clinical experiences using a 0.5 T open MR system.
J Magn Reson Imaging. 2002 Nov;16(5):576-83.

30- Morikawa S, Inubushi T, Kurumi Y, Naka S, Sato K, Tani T, Haque HA, Tokuda J, Hata N.
New assistive devices for MR-guided microwave thermocoagulation of liver tumors.
Acad Radiol. 2003 Feb;10(2):180-8.

31- Morikawa S, Inubushi T, Kurumi Y, Naka S, Sato K, Demura K, Tani T, Haque HA, Tokuda J, Hata N.
Advanced computer assistance for magnetic resonance-guided microwave thermocoagulation of liver tumors.
Acad Radiol. 2003 Dec;10(12):1442-9.

32- J. Xu, X. Yang, D. Wu, K. Chen, H. Ren, and P. Liang, "An efficient needle insertion robotics system for ultrasound-guided hepatic microwave coagulation therapy," in *Automation and Logistics, 2007 IEEE International Conference on*, 2007, pp. 1258-1261

33- Hoffmann R, Rempp H, Keßler DE, Weiß J, Pereira PL, Nikolaou K, Clasen S.
R-guided microwave ablation in hepatic tumours: initial results in clinical routine.
Eur Radiol. 2017 Apr;27(4):1467-1476.

34- G. Biffi Gentili, C. Ignesti, and V. Tesi
Development of a novel switched-mode 2.45 GHz microwave multiapplicator ablation system
International Journal of Microwave Science and Technology, vol. 2014, 2014

35- Biffi Gentili G, Ignesti C.
Dual applicator thermal ablation at 2.45 GHz: a numerical comparison and experiments on synchronous versus asynchronous and switched-mode feeding.
Int J Hyperthermia. 2015;31(5):528-37.

36-Francone E,Muzio E, D'Ambra L,Aschele C, Stefanini T, Sani C, Falco E, Berti S
Precoagulation-assisted parenchyma-sparing laparoscopic liver surgery: rationale and surgical technique.
Surg Endosc. 2017 Mar;31(3):1354-1360.

37- Percivale A, Griseri G, Gastaldo A, Benasso M, Pellicci R.
Microwave assisted liver resection: clinical feasibility study and preliminary results.
Minerva Chir. 2012 Oct;67(5):415-20.

38- Adebar TK, Greer JD, Laeseke PF, Hwang GL, Okamura AM.
Methods for Improving the Curvature of Steerable Needles in Biological Tissue.
IEEE Trans Biomed Eng. 2016 Jun;63(6):1167-77

39- Dimitri M, Staderini F, Brancadoro M, Frosini F, Coratti A, Capineri L, Corvi A, Cianchi F, Biffi Gentili G.
A new microwave applicator for laparoscopic and robotic liver resection.
Int J Hyperthermia. 2019;36(1):75-86.

40- Available: https://github.com/jhu-dvrk/sawIntuitiveResearchKit/wiki